

Inverse magnetic energy cascades embedded in magnetohydrodynamical turbulence

NICHOLAS M. RATHMANN¹ AND PETER D. DITLEVSEN¹

¹*Niels Bohr Institute, University of Copenhagen, Denmark*

(Received —; Revised —; Accepted —)

Submitted to ApJ

ABSTRACT

The existence of partially conserved enstrophy-like quantities is conjectured to cause embedded, inverse magnetic energy cascades to develop in magnetohydrodynamical (MHD) turbulence. By decomposing the velocity and magnetic fields in spectral space onto helical modes, we show that two new quantities exist which are partially conserved among a set of three-wave (triad) interactions in MHD turbulence. In a subset of these helical triad interactions, the quantities become enstrophy-like, which, by analogy to enstrophy-conserving triad interactions in two-dimensional, nonconducting hydrodynamical turbulence, are conjectured to cause embedded, inverse magnetic energy cascades to develop. We test the resulting predictions by constructing a nonlocal helical MHD shell model (reduced wave-space numerical model) of the minimal set of triad interactions (MTIs) required to conserve the ideal MHD invariants, energy, magnetic helicity, and cross-helicity. The numerically simulated MTIs demonstrate that, for a range of forcing configurations, the partial invariants are indeed useful for understanding the embedded energy cascade contributions to the total spectral energy flux, which has potential implications for the turbulent dynamo action, central to the evolution of astrophysical magnetic fields.

Keywords: MHD turbulence, energy cascade, helical decomposition, triad interactions, pseudo-invariants, dynamo

1. INTRODUCTION

A central problem in astrophysics is how large-scale magnetic fields are generated by astrophysical bodies such as planets, stars and galaxies. A popular explanation is that a dynamo action occurs, whereby a magnetic seed field is amplified by interacting with the velocity field inside the electroconducting fluid of the body (Moffatt 1978; Brandenburg & Subramanian 2005). That is, magnetic energy grows by feeding of kinetic energy until reaching a point of saturation, given that the conversion rate of kinetic to magnetic energy is greater than the Joule dissipation rate. A celebrated example is the α -effect in mean-field dynamo theory, which explains the development of large-scale magnetic fields provided that the flow possesses kinetic helicity (handedness) (Steenbeck et al. 1966; Moffatt 1978; Krause & Rädler 1980). More recently, however, the upscale cascade of the magnetic helicity (Frisch et al. 1975; Pouquet et al. 1976; Biskamp 1993), an inviscid integral of motion in magnetohydrodynamical (MHD)

turbulence, has received a lot of attention for its role in turbulent dynamos (Brandenburg & Subramanian 2005; Alexakis et al. 2006; Stepanov et al. 2014; Linkmann & Dallas 2016, 2017; Linkmann et al. 2017) because of the implied upscale (from small to larger scales) transfer of magnetic energy due to the spectral bounds between magnetic energy and magnetic helicity (Moffatt 1978; Biskamp 1993).

In an attempt to better understand the turbulent dynamo action, it is therefore central to study the nonlinear dynamics by which inviscid invariants are transferred across spatial scales in order to cast light on the evolution of planetary and stellar magnetic fields.

In three-dimensional (3D), isotropic, nonconducting hydrodynamical (HD) turbulence, kinetic energy, on average, cascades from the large integral (forcing) scale of motion to the small, dissipative Kolmogorov scale (where dissipated as heat), synonymous with a forward or direct energy cascade. In naturally occurring HD turbulence, however, such as two-dimensional (2D) flows (Boffetta & Musacchio 2010; Mininni & Pouquet 2013) and strongly rotating 3D flows with a broken mirror symmetry (Sulem et al. 1989; Mininni et al.

2009), an upscale cascade of energy has been found to occur, synonymous with an inverse or reverse energy cascade.

In 3D HD turbulence, the production of enstrophy (vorticity squared), by means of the stretching and bending term in the Navier–Stokes equation, allows for the dissipation of energy at the Kolmogorov scale. In 2D HD turbulence, the stretching and bending term is however absent, and enstrophy is too inviscidly conserved like energy and can only grow by increased pumping. Because the relative dissipation of enstrophy to energy increases with Reynolds number (decreasing Kolmogorov scale), the reversed (upscale) energy cascade in 2D may therefore be understood in terms of the conservation of enstrophy effectively blocking the forward cascade of energy.

An analogous explanation for the energy cascade reversals in 3D HD turbulence is less developed and more subtle in comparison. In 3D HD flows, a second inviscid invariant also exists: kinematic helicity, defined as the integral of the inner product between velocity and vorticity (Moffatt 1969; Kraichnan 1973; Brissaud et al. 1973). In contrast to enstrophy in 2D, the effect of helicity on the directionality of the energy cascade in 3D is less understood. Although the relative dissipation of helicity to energy also increases with Reynolds number, helicity is not sign definite as opposed to enstrophy. Consequently, a concurrent forward energy cascade and increased dissipation with Reynolds number of both signs of helicity is possible, as long as no net helicity production occurs (note the dissipation of one sign of helicity results in the production of the opposite sign) (Ditlevsen & Giuliani 2001a).

By decomposing the velocity field in spectral space onto helical modes (spectral-helical basis), each velocity mode evolves by helical three-wave (triad) interactions (Constantin & Majda 1988; Waleffe 1992). Recently, new quantities were identified in 3D HD turbulence which are partially conserved among helical triad interactions (Biferale et al. 2012; De Pietro et al. 2015; Rathmann & Ditlevsen 2017), henceforth also referred to as *pseudo-invariants*. In a subset of helical triad interactions, these pseudo-invariants become enstrophy-like (Rathmann & Ditlevsen 2017), and have been associated with reversed energy cascades developing (Biferale et al. 2012; De Pietro et al. 2015; Rathmann & Ditlevsen 2017). It is therefore possible that embedded (hidden), reverse energy cascades might generally exist in 3D HD turbulence due to partial invariants with implications for the net transfer of energy.

Because of their clear physical interpretation, quadratic invariants, such as enstrophy, play a central role in the study of turbulent cascade dynamics. In this work, we conjecture that the spectral-helically decomposed energy cascade in ideal MHD turbulence might too be understood in terms of pseudo-invariants, which has potential implications for the large-scale

dynamo action. We show that two new enstrophy-like quantities are partially conserved by the ideal MHD equations, and argue that embedded, inverse magnetic energy cascades might develop as a result. By constructing a nonlocal helical MHD shell model (reduced wave-space model), we find that the new pseudo-invariants are indeed useful for understanding the simulated energy cascade partitioning between helical triad interactions, supporting the possibility of embedded inverse magnetic energy cascades.

2. THE SPECTRAL-HELICAL DECOMPOSITION

In real-space, the incompressible, ideal MHD equations are

$$\begin{aligned} (\partial_t - \nu \nabla^2) \mathbf{u} &= -(\mathbf{u} \cdot \nabla) \mathbf{u} + (\nabla \times \mathbf{B}) \times \mathbf{B} - \nabla p \\ (\partial_t - \eta \nabla^2) \mathbf{B} &= (\mathbf{B} \cdot \nabla) \mathbf{u} - (\mathbf{u} \cdot \nabla) \mathbf{B} \\ \nabla \cdot \mathbf{u} &= 0 \quad \text{and} \quad \nabla \cdot \mathbf{B} = 0, \end{aligned} \quad (1)$$

where \mathbf{u} is the velocity field, \mathbf{B} the magnetic field in Alfvén units, ν is the kinematic viscosity, η the magnetic resistivity, p the pressure, and the density set to $\rho = 1$ for convenience. In spectral space, the divergence-free constraints on \mathbf{u} and \mathbf{B} translate into $\mathbf{k} \cdot \mathbf{u}(\mathbf{k}) = 0$ and $\mathbf{k} \cdot \mathbf{B}(\mathbf{k}) = 0$. The helical basis (Constantin & Majda 1988; Waleffe 1992) exploits this property by decomposing each complex spectral component into two helical modes, $\mathbf{h}_{\pm}(\mathbf{k})$, which are mutually perpendicular to \mathbf{k} and are eigenmodes of the curl operator, i.e. $i\mathbf{k} \times \mathbf{h}_{\pm} = \pm k \mathbf{h}_{\pm}$, where $k = |\mathbf{k}|$. In this basis, the velocity and magnetic components are given by

$$\begin{aligned} \mathbf{u}(\mathbf{k}) &= u_+(\mathbf{k}) \mathbf{h}_+ + u_-(\mathbf{k}) \mathbf{h}_- \\ \mathbf{B}(\mathbf{k}) &= B_+(\mathbf{k}) \mathbf{h}_+ + B_-(\mathbf{k}) \mathbf{h}_-, \end{aligned}$$

and the ideal MHD invariants energy (E), magnetic helicity (H_M), and cross helicity (H_C), are given by

$$E = \sum_{\mathbf{k}} (|u_+(\mathbf{k})|^2 + |u_-(\mathbf{k})|^2 + |B_+(\mathbf{k})|^2 + |B_-(\mathbf{k})|^2) \quad (2)$$

$$H_M = \sum_{\mathbf{k}} k^{-1} (|B_+(\mathbf{k})|^2 - |B_-(\mathbf{k})|^2) \quad (3)$$

$$H_C = \sum_{\mathbf{k}} (u_+(\mathbf{k}) B_+^*(\mathbf{k}) + u_-(\mathbf{k}) B_-^*(\mathbf{k}) + \text{c.c.}). \quad (4)$$

Lessinnes et al. (2009) first proposed applying the decomposition to the MHD equations (1) too, giving

$$(\partial_t + \nu k^2) u_s(\mathbf{k}) = \quad (5)$$

$$\begin{aligned} &\sum_{\mathbf{k}+\mathbf{k}'+\mathbf{k}''=0} \left(\sum_{s',s''} (s'k' - s''k'') g_{ss's''} u_{s'}^*(\mathbf{k}') u_{s''}^*(\mathbf{k}'') \right. \\ &\quad \left. - \sum_{\sigma',\sigma''} (\sigma'k' - \sigma''k'') g_{s\sigma'\sigma''} B_{\sigma'}^*(\mathbf{k}') B_{\sigma''}^*(\mathbf{k}'') \right) \end{aligned}$$

$$(\partial_t + \eta k^2) B_{\sigma}(\mathbf{k}) = \sigma k \sum_{\mathbf{k}+\mathbf{k}'+\mathbf{k}''=0} \quad (6)$$

$$\sum_{\sigma',s''} g_{\sigma\sigma's''} B_{\sigma'}^*(\mathbf{k}') u_{s''}^*(\mathbf{k}'') - \sum_{s',\sigma''} g_{\sigma s'\sigma''} u_{s'}^*(\mathbf{k}') B_{\sigma''}^*(\mathbf{k}''),$$

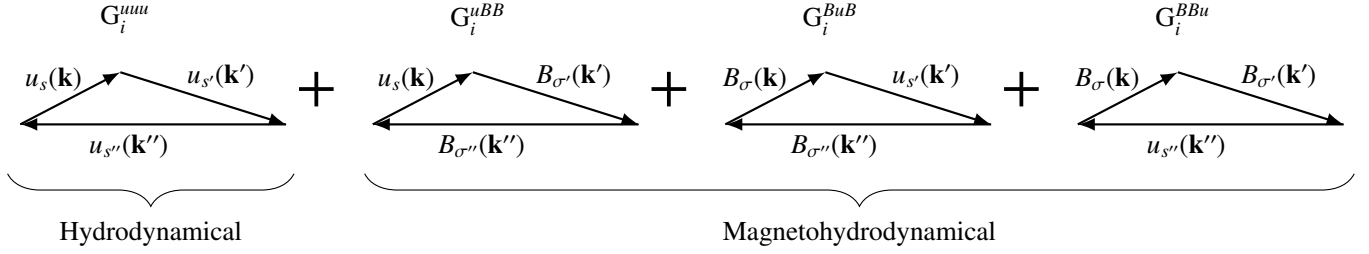


Figure 1. The minimal set of helical triad interactions (MTI) required to conserve all three magnetohydrodynamical invariants, energy (E), magnetic helicity (H_M), and cross-helicity (H_C). For a given triad of waves, $\{\mathbf{k}, \mathbf{k}', \mathbf{k}''\}$, the MTI consists of four (triad) components per possible combination of helical signs of the interacting modes $\{s, s', s'', \sigma, \sigma', \sigma''\}$ (or sign group numbers i , see text): one hydrodynamical (HD) helical triad interaction (G_i^{uuu}) and three magnetohydrodynamical (MHD) helical triad interactions (G_i^{uBB} , G_i^{BuB} , G_i^{BBu}). The behaviour of the four MTI components is proposed to be explained by the conservation (or lack thereof) of an enstrophy-like pseudo-invariant quantity, $E^{(\alpha)}$.

where $\{s, s', s'', \sigma, \sigma', \sigma''\} = \pm 1$ are helical sign coefficients of the interacting helical modes, and

$$g_{ss's''} = -1/4 \mathbf{h}_{s'}^*(\mathbf{k}') \times \mathbf{h}_{s''}^*(\mathbf{k}'') \cdot \mathbf{h}_s^*(\mathbf{k})$$

is an interaction coefficient. Velocity modes $u_s(\mathbf{k})$ thus evolve by helical triad (three-wave) interactions involving $\{u_{s'}(\mathbf{k}'), u_{s''}(\mathbf{k}'')\}$ and $\{B_{\sigma'}(\mathbf{k}'), B_{\sigma''}(\mathbf{k}'')\}$, while magnetic modes $B_{\sigma}(\mathbf{k})$ evolve by helical triad interactions involving $\{u_{s'}(\mathbf{k}'), B_{\sigma''}(\mathbf{k}'')\}$ and $\{B_{\sigma'}(\mathbf{k}'), u_{s''}(\mathbf{k}'')\}$, provided that triads close ($\mathbf{k} + \mathbf{k}' + \mathbf{k}'' = 0$).

For each of the four types of helical triad interactions, $2^3 = 8$ distinct combinations of helical signs are possible as indicated by the sums over helical signs in (5)–(6). If sorted against shared interaction coefficients, however, only four unique sign combinations remain per triad type: for each of the triad types $\{u_s(\mathbf{k}), u_{s'}(\mathbf{k}'), u_{s''}(\mathbf{k}'')\}$, $\{u_s(\mathbf{k}), B_{\sigma'}(\mathbf{k}'), B_{\sigma''}(\mathbf{k}'')\}$, $\{B_{\sigma}(\mathbf{k}), u_{s'}(\mathbf{k}'), B_{\sigma''}(\mathbf{k}'')\}$, and $\{B_{\sigma}(\mathbf{k}), B_{\sigma'}(\mathbf{k}'), u_{s''}(\mathbf{k}'')\}$, the associated helical signs $\{s, s', s''\}$, $\{s, \sigma', \sigma''\}$, $\{\sigma, s', \sigma''\}$, and $\{\sigma, \sigma', s''\}$, respectively, may be any one of the combinations $\pm\{+, -, +\}$, $\pm\{+, -, -\}$, $\pm\{+, +, -\}$, and $\pm\{+, +, +\}$. From here on, these four possible combinations of helical signs shall be referred to as sign groups $i = 1, 2, 3, 4$, respectively. Any particular helical triad interaction may therefore be referred to by a combination of the triad type and its sign group number, henceforth denoted compactly by G_i^{XYZ} . In this notation, i refers to the sign group number, and X, Y and Z are placeholders for the fields of the interacting modes. Note that only the four types $XYZ \in \{uuu, uBB, BuB, BBu\}$ exist, and that X is the field associated with wave-vector \mathbf{k} , Y with \mathbf{k}' , and Z with \mathbf{k}'' .

Isolating terms in (5)–(6) involving a single triad of waves, $\{\mathbf{k}, \mathbf{k}', \mathbf{k}''\}$, only four triad interactions (components) remain per possible combination of helical signs, namely $G_i^{uuu} + G_i^{uBB} + G_i^{BuB} + G_i^{BBu}$, hereafter referred to as a minimal set of triad interactions (MTI) following Linkmann et al. (2017) (Figure 1). Note that $2^6 = 64$ distinct MTIs are possible, and that only in the case of homochiral MTIs ($s = \sigma$, $s' = \sigma'$, and $s'' = \sigma''$) do the MTI components share sign group numbers (i).

By noting the cyclic property of $g_{ss's''}$, the evolution of velocity and magnetic modes in a given MTI is governed by (Linkmann et al. 2016)

$$\begin{aligned} d_t u_s &= (s'k' - s''k'')g_{ss's''}u_{s'}^*u_{s''}^* - (\sigma'k' - \sigma''k'')g_{s\sigma'\sigma''}B_{\sigma'}^*B_{\sigma''}^* \\ d_t u_{s'} &= (s''k'' - sk)g_{ss's''}u_s^*u_{s''}^* - (\sigma''k'' - \sigma k)g_{\sigma s'\sigma''}B_{\sigma'}^*B_{\sigma''}^* \\ d_t u_{s''} &= (sk - s'k')g_{ss's''}u_s^*u_{s'}^* - (\sigma k - \sigma'k')g_{\sigma\sigma's'}B_{\sigma'}^*B_{\sigma''}^* \\ d_t B_{\sigma} &= \sigma k (g_{\sigma\sigma's'}B_{\sigma'}^*u_{s''}^* - g_{\sigma s'\sigma''}u_{s'}^*B_{\sigma''}^*) \\ d_t B_{\sigma'} &= \sigma'k' (g_{\sigma s'\sigma''}B_{\sigma''}^*u_s^* - g_{\sigma\sigma's'}u_s^*B_{\sigma'}^*) \\ d_t B_{\sigma''} &= \sigma''k'' (g_{\sigma s'\sigma''}B_{\sigma'}^*u_{s'}^* - g_{s\sigma'\sigma''}u_{s'}^*B_{\sigma''}^*), \end{aligned} \quad (7)$$

where the compact notations $u_s = u_s(\mathbf{k})$, $u_{s'} = u_{s'}(\mathbf{k}')$, and $u_{s''} = u_{s''}(\mathbf{k}'')$ are used (and likewise for B). From this simpler form of the spectral dynamics, it immediately follows that each MTI conserves energy, magnetic helicity and cross-helicity, by

$$\begin{aligned} d_t [E(\mathbf{k}) + E(\mathbf{k}') + E(\mathbf{k}'')] &= 0 \\ d_t [H_M(\mathbf{k}) + H_M(\mathbf{k}') + H_M(\mathbf{k}'')] &= 0 \\ d_t [H_C(\mathbf{k}) + H_C(\mathbf{k}') + H_C(\mathbf{k}'')] &= 0, \end{aligned}$$

respectively, where $E(\mathbf{k}) = |u_+(\mathbf{k})|^2 + |u_-(\mathbf{k})|^2 + |B_+(\mathbf{k})|^2 + |B_-(\mathbf{k})|^2$, $H_M(\mathbf{k}) = k^{-1}(|B_+(\mathbf{k})|^2 - |B_-(\mathbf{k})|^2)$, and $H_C(\mathbf{k}) = u_+(\mathbf{k})B_+(\mathbf{k}) + u_-(\mathbf{k})B_-(\mathbf{k}) + \text{c.c.}$. The ideal MHD invariants (2)–(4) are thus conserved per triad of waves, but only collectively by the four components $G_i^{uuu} + G_i^{uBB} + G_i^{BuB} + G_i^{BBu}$ constituting a MTI (for any choice of helical signs), hence the notion of a minimal set.

The existence of three invariants makes understanding and predicting the details of the energy cascade in ideal MHD turbulence particularly challenging (Iroshnikov 1964; Matthaeus & Zhou 1989; Boldyrev 2005). While the relative magnitudes of energy, magnetic helicity, and cross-helicity fluxes between the three triad legs are fixed and determined by the coefficients in (7), the magnitudes and directions of the average fluxes (to or from a leg) depend on the unknown triple-correlators $\langle u_{s'}^*u_s^*u_{s''}^* \rangle + \text{c.c.}$, $\langle u_{s'}^*B_{\sigma'}^*B_{\sigma''}^* \rangle + \text{c.c.}$, $\langle B_{\sigma'}^*u_{s'}^*B_{\sigma''}^* \rangle + \text{c.c.}$, and $\langle B_{\sigma'}^*B_{\sigma''}^*u_{s'}^* \rangle + \text{c.c.}$.

Linkmann et al. (2016) recently proposed the behaviour of a given MTI might be understood from the linear stability of (7) around trivial steady-states, inspired by a similar approach in HD turbulence (Waleffe 1992). Waleffe (1992) suggested that energy, on average, flows from the most unstable triad leg (mode) and in to the other two. In this regard, the behaviour of a given triad may be classified as either forward (F-class) if the smallest wave-number mode (largest scale) is linearly unstable, suggesting that energy is transferred to the two smaller scales (forward cascade), or reverse (R-class) if either the middle or smallest wave-number modes are unstable, suggesting that energy is transferred either partly or fully to larger scales (reverse cascade), respectively. By considering the linear stability of the states $\{u_s^*, u_{s'}^*, u_{s''}^*, B_\sigma^*, B_{\sigma'}^*, B_{\sigma''}^*\} = \{u_0, 0, 0, B_0, 0, 0\}, \{0, u_0, 0, 0, B_0, 0\}, \{0, 0, U_0, 0, 0, B_0\}$, where u_0 and B_0 are constants, Linkmann et al. (2016) showed that the modes $x_i = (u_s, B_\sigma)$ evolve by $\ddot{x}_i = M_{ij}x_j$ [and similarly for $x_i = (u_{s'}, B_{\sigma'}), (u_{s''}, B_{\sigma''})$], but with different M_{ij} . The modal (leg) stabilities therefore depend on the existence of M_{ij} eigenvalues with real, positive parts, which have complicated dependencies compared to the HD case: in addition to M_{ij} depending on the helical signs of the three interacting modes, such as a stability analysis of the pure HD case also does, it moreover depends on the ratio u_0/B_0 , and the alignment between velocity and magnetic modes (cross-helicity).

In fully developed MHD turbulence, it is, however, not clear to what extent a linear stability analysis is relevant for the evolution of velocity and magnetic fields. The stability analysis is based on the behaviour of a single MTI around states unlikely to be generally realized in physical flows, and the predicted behaviours have yet to be attributed any physical mechanisms.

3. THE PSEUDO-INVARIANTS

In HD turbulence, quadratic invariants play a fundamental role in the understanding of turbulent cascade dynamics, such the energy cascade reversal in 2D which may straightforwardly be understood in terms of the differential dissipation of enstrophy compared to energy. The recent discovery that G_4^{uuu} interactions in 3D separately conserve both signs of kinematic helicity was proposed to explain the R-class nature of G_4^{uuu} interactions in analogy to enstrophy-conserving interactions in 2D (Biferale et al. 2012). More recently, the mixed forward–reverse behaviour by G_2^{uuu} interactions depending on triad geometry (Waleffe 1992; De Pietro et al. 2015; Rathmann & Ditlevsen 2017) was also proposed to be explained by the existence of a new enstrophy-like invariant $E^{(\alpha)}(\mathbf{k}) = k^\alpha (|u_+(\mathbf{k})|^2 + |u_-(\mathbf{k})|^2)$, where $\alpha \in \mathbb{R}$ depends on the specific triad shape $\{k, k', k''\}$ (Rathmann & Ditlevsen 2017).

Following Rathmann & Ditlevsen (2017), we here show that a subset of MHD triad interactions exist which too conserve

enstrophy-like quantities, which might help understand the behaviour of MTIs in terms of conserved quantities in analogy to enstrophy-conserving interactions in 2D HD turbulence. Inspired by the HD pseudo-invariant, consider therefore the generalized spectral energy density defined as

$$E^{(\alpha)}(\mathbf{k}) = k^\alpha (|u_+(\mathbf{k})|^2 + |u_-(\mathbf{k})|^2 + |B_+(\mathbf{k})|^2 + |B_-(\mathbf{k})|^2). \quad (8)$$

This quantity is thus enstrophy-like for exponents $\alpha > 0$, and might induce an energy cascade reversal if conserved by triad interactions. Note that $\alpha = 0$ corresponds to energy which is conserved by any MTI.

Applying (7) to (8), it follows that the pseudo-invariant is conserved if $d_t[E^{(\alpha)}(\mathbf{k}) + E^{(\alpha)}(\mathbf{k}') + E^{(\alpha)}(\mathbf{k}'')] = 0$, implying

$$\begin{aligned} k^{\alpha+1} [& L^{uuu}(\alpha) g_{ss's''} u_s^* u_{s'}^* u_{s''}^* - L^{uBB}(\alpha) g_{\sigma\sigma'\sigma''} u_s^* B_{\sigma'}^* B_{\sigma''}^* \\ & - L^{BuB}(\alpha) g_{\sigma s' \sigma''} B_{\sigma'}^* u_{s'}^* B_{\sigma''}^* + L^{BBu}(\alpha) g_{\sigma\sigma' s''} B_{\sigma'}^* B_{\sigma''}^* u_{s''}^*] \\ & + \text{c.c.} = 0, \end{aligned}$$

where [suppressing dependencies on wave-numbers and helical signs in the definitions of $L^{XYZ}(\alpha)$]

$$\begin{aligned} L^{uuu}(\alpha) = & \left(s' \frac{k'}{k} - s'' \frac{k''}{k} \right) + \left(s'' \frac{k''}{k} - s \right) \left(\frac{k'}{k} \right)^\alpha + \left(s - s' \frac{k'}{k} \right) \left(\frac{k''}{k} \right)^\alpha \quad (9) \end{aligned}$$

$$L^{uBB}(\alpha) = \left(\sigma' \frac{k'}{k} - \sigma'' \frac{k''}{k} \right) - \sigma' \left(\frac{k'}{k} \right)^{\alpha+1} + \sigma'' \left(\frac{k''}{k} \right)^{\alpha+1} \quad (10)$$

$$L^{BuB}(\alpha) = \sigma + \left(\sigma'' \frac{k''}{k} - \sigma \right) \left(\frac{k'}{k} \right)^\alpha - \sigma'' \left(\frac{k''}{k} \right)^{\alpha+1} \quad (11)$$

$$L^{BBu}(\alpha) = \sigma - \sigma' \left(\frac{k'}{k} \right)^{\alpha+1} + \left(\sigma' \frac{k'}{k} - \sigma \right) \left(\frac{k''}{k} \right)^\alpha. \quad (12)$$

Conservation by a MTI thus requires the existence of solutions $\alpha \in \mathbb{R}$ which simultaneously fulfil $L^{XYZ}(\alpha) = 0$ for all $XYZ \in \{uuu, uBB, BuB, BBu\}$. Since this is not possible, we are here interested in the possibility that the four individual MTI components might separately conserve different pseudo-invariants, leading to embedded, component-wise reversals of the energy cascade.

Equations (9)–(12) are functions of the wavenumber ratios, k'/k and k''/k , and consist of a constant term and two monotonically increasing or decreasing terms. For solutions $L^{XYZ}(\alpha) = 0$ to exist besides energy ($\alpha = 0$), the signs of the three terms in each of (9)–(12) must alternate (considering the ordering $k \leq k' \leq k''$ without loss of generality). On inspection, it follows that only interactions $G_i^{XYZ} \in \{G_2^{uuu}, G_2^{BuB}, G_3^{BuB}, G_3^{BBu}, G_4^{BBu}\}$ solve $L^{XYZ}(\alpha) = 0$ for $\alpha \neq 0$.

The HD pseudo-invariant conservation by G_2^{uuu} interactions has previously been investigated (De Pietro et al. 2015; Rathmann & Ditlevsen 2017), finding a cascade reversal

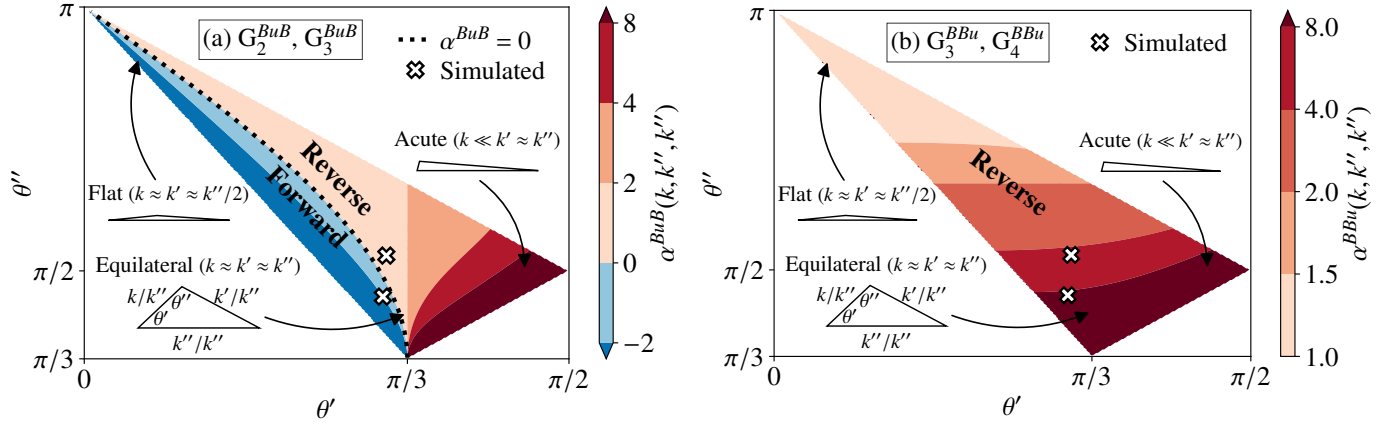


Figure 2. Magnetohydrodynamical helical triad interactions conserving enstrophy-like pseudo-invariants. The behaviours of triad interactions G_2^{BuB}, G_3^{BuB} (panel a), and G_3^{BBu}, G_4^{BBu} (panel b) are proposed to be explained by the conservation of a pseudo-invariant, $E^{(\alpha)}$, which depends on triad geometry. Panels a and b show in red colors the subset of triad geometries conserving an enstrophy-like pseudo-invariant [exponents $\alpha^{BuB}(k, k', k'') > 0$ and $\alpha^{BBu}(k, k', k'') > 0$], which are conjectured to cause reverse energy cascade contributions to develop. The black dotted line in panel a shows the analytical transition line which separates the forward and reverse cascade contributions by G_2^{BuB} and G_3^{BuB} interactions [equation (13)]. Crosses mark the triad geometries considered in numerical simulations.

indeed takes place for a nonlocal subset of triad geometries due to the invariant becoming enstrophy-like ($\alpha > 0$). The pseudo-invariant conservations by MHD interactions $G_2^{BuB}, G_3^{BuB}, G_3^{BBu}$, and G_4^{BBu} have, however, not previously been considered. Unlike the G_2^{uuu} pseudo-invariant, the MHD pseudo-invariants do not depend on the helical signs of all three triad legs (modes): the helical sign of the velocity mode does not enter (10)–(12), implying G_2^{BuB} and G_3^{BuB} share the same pseudo-invariants, as do G_3^{BBu} and G_4^{BBu} .

Figures 2a and 2b show the numerical solutions w.r.t. α for $L^{BuB}(\alpha) = 0$ and $L^{BBu}(\alpha) = 0$, respectively, hereafter referred to as α^{BuB} and α^{BBu} . The solutions are shown for all possible (noncongruent) triad geometries (coloured area) by expressing each triad in terms of the two interior angles θ' and θ'' using the Sine rule: $k'/k = \sin(\theta')/\sin(\pi - \theta' - \theta'')$ and $k''/k = \sin(\theta'')/\sin(\pi - \theta' - \theta'')$. Figure 2a shows that G_2^{BuB} and G_3^{BuB} interactions may, similarly to G_2^{uuu} , contribute either to a forward cascade in a F-class fashion ($\alpha^{BuB} < 0$, blue colors) or reversely in a R-class fashion ($\alpha^{BuB} > 0$, red colors). The exact transition line through the space of triad geometries separating the two behaviours is given by $dL^{BuB}(\alpha)/d\alpha|_{\alpha=0} = 0$, yielding

$$\log k'/k = \frac{\log k''/k}{1 - \sigma\sigma''k/k''}, \quad (13)$$

which corresponds to the geometries for which the energy and pseudo-invariant solutions collapse (Figure 2a, black dotted line). Figure 2b, on the other hand, shows that G_3^{BBu} and G_4^{BBu} interactions always conserve an enstrophy-like quantity ($\alpha^{BBu} > 0$) regardless of triad geometry, suggesting they should contribute with a reverse energy cascade component in a R-class fashion.

Note, importantly, that G_3^{BBu} and G_4^{BBu} interactions may be associated with reverse magnetic energy transfers since

both the largest and middle triad legs are magnetic, whereas G_2^{BuB} and G_3^{BuB} interactions have a velocity component as the middle triad leg, implying the reversed energy cascade might only in part be magnetic.

We have thus arrived at several specific, testable predictions for the behaviours of the energy cascade contributions from the four individual MTI components: (i) G_i^{uBB} triads contribute to a forward cascade (for all sign groups $i = 1, 2, 3, 4$), (ii) G_1^{BuB} and G_4^{BuB} contribute to a forward cascade while G_2^{BuB} and G_3^{BuB} may contribute either to a forward or reverse cascade depending on triad geometry, and (iii) G_1^{BBu} and G_2^{BBu} contribute to a forward cascade while G_3^{BBu} and G_4^{BBu} contribute reversely.

4. THE MTI SHELL MODEL

To test the pseudo-invariant based predictions, we constructed a MTI shell model (reduced wave-space model). Shell models have previously provided valuable insight into the spectral cascade dynamics of MHD turbulence (Lessinnes et al. 2009; Plunian et al. 2013), and are especially convenient in MHD turbulence due to the added number of nonlinear interactions (Figure 1) making direct numerical simulations computationally expensive. Only relatively recently have direct numerical simulations of (5)–(6) been conducted giving insight into the behaviour of helical MHD triad dynamics and the role of the ideal MHD invariants in the spectral-helical basis (Linkmann & Dallas 2017; Linkmann et al. 2017).

Shell models allow simulating very long inertial ranges at the expense of severely truncating spectral space: only wave-numbers distributed exponentially according to $k_n = k_0\lambda^n$ are retained, where $n = 0, \dots, N$ are the shell indices, $k_0 \in \mathbb{R}_+$, and $\lambda \in]1, (1 + \sqrt{5})/2] =]1, \varphi]$. The golden ratio φ is the upper limit such that any set of nearest neighbour waves fulfil the triangle inequality as required by (5)–(6). All

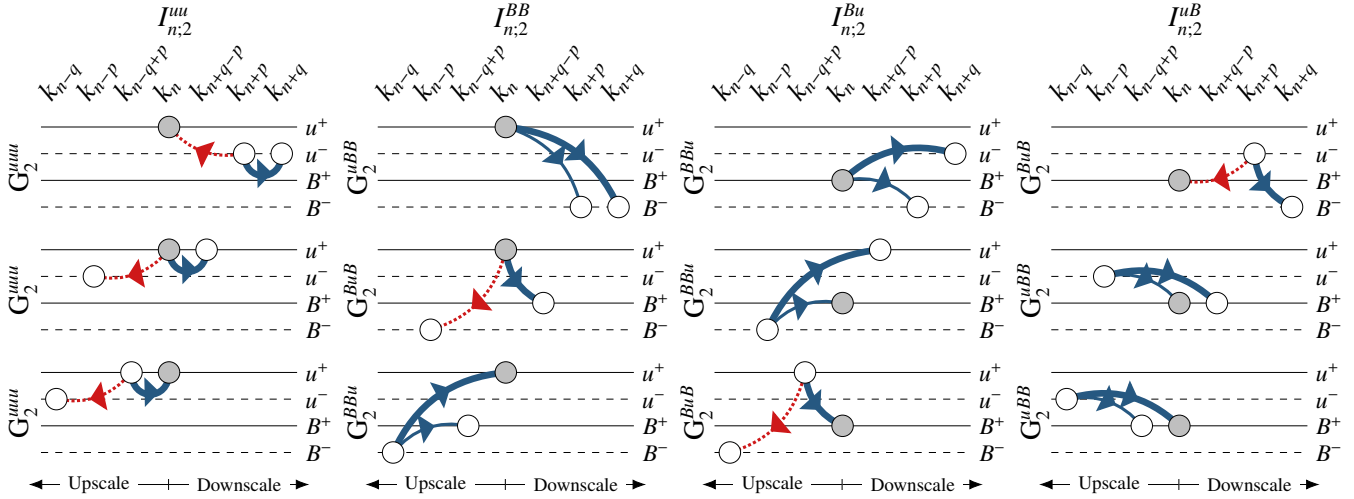


Figure 3. The three helical triad interactions per shell model term $I_{n;i}^{uu}$, $I_{n;i}^{BB}$, $I_{n;i}^{Bu}$, and $I_{n;i}^{uB}$ for sign group $i = 2$. Only interactions coupling to u_n^+ or B_n^+ (filled gray circles) are shown, complementary interactions coupling to u_n^- or B_n^- are given by similar but sign-flipped interactions. While the terms $I_{n;i}^{BB}$, $I_{n;i}^{Bu}$, and $I_{n;i}^{uB}$ each contain a mix of the three MHD MTI components (G_i^{uBB} , G_i^{BuB} , and G_i^{BBu}), the term $I_{n;i}^{uu}$ contains only HD components (G_i^{uuu}). Arrows indicate the average energy transfer directions predicted from the pseudo-invariant conservations combined with (7) (fixing the relative leg-to-leg transfer magnitudes): solid blue (dashed red) arrows denote forward (reverse) energy transfers, while thick (thin) arrows represent dominant (subordinate) transfers. Note that the behaviours of G_2^{uuu} and G_2^{uBB} interactions are here shown assuming local triad geometries (dominant forward cascade).

spectral components are generally reduced to depend only on wave magnitudes expect for a few cases (Gürçan 2017; Monthus 2018; Gürçan 2018), and shell models may therefore be regarded as simple, structureless cascade models.

The pioneering work on constructing helical shell models was done by Benzi et al. (1996), which, since then, has inspired other helical shell models and led to important insights on helically decomposed triad dynamics of HD turbulence (Ditlevsen & Giuliani 2001a,b; Lessinnes et al. 2011; De Pietro et al. 2015; Rathmann & Ditlevsen 2016; Sahoo et al. 2017; De Pietro et al. 2017) and MHD turbulence (Lessinnes et al. 2009; Plunian et al. 2013; Stepanov et al. 2015). Following Rathmann & Ditlevsen (2016) for the Navier–Stokes equations, (5)–(6) may similarly be cast into a shell model by noting the MHD triadic interaction structure is similar but with different interaction coefficients. Considering only homochiral MTIs (elaborated on below) with fixed shape triads (fixed interior angles) and adopting the usual shorthand notations $u_n^s = u_s(k_n)$ and $B_n^s = B_s(k_n)$, the shell model for a single kind of MTI is given by

$$(d_t + D_n^u) u_n^s = sk_n \left[I_{n;i}^{uu} \left(1, \frac{\epsilon_i}{\lambda^p}, \frac{\xi_i}{\lambda^q} \right) - I_{n;i}^{BB} \left(1, \frac{\epsilon_i}{\lambda^p}, \frac{\xi_i}{\lambda^q} \right) \right] + f_n^u \quad (14)$$

$$(d_t + D_n^B) B_n^s = sk_n \left[I_{n;i}^{Bu} (\tau_i, \tau_i, \tau_i) - I_{n;i}^{uB} (\tau_i, \tau_i, \tau_i) \right] + f_n^B, \quad (15)$$

where the resolved triad interactions are collected in $I_{n;i}^{VW}$, defined as

$$I_{n;i}^{VW} (a, b, c) = aV_{n+p}^{s,s_i^*,s_i'} W_{n+q}^{s,s_i^*,s_i'} - bV_{n-p}^{s,s_i^*,s_i'} W_{n-p+q}^{s,s_i^*,s_i'} + cV_{n-q}^{s,s_i^*,s_i'} W_{n-q+p}^{s,s_i^*,s_i'}$$

Here, the helical signs of each sign group are for convenience referred to by $\{s, s', s''\} = \pm\{+, s_i', s_i''\}$, such that $\{s_i', s_i''\} = \{-, +\}, \{-, -\}, \{+, -\}, \{+, +\}$ for groups $i = 1, 2, 3, 4$, respectively, and the interactions coefficients are given by

$$\begin{aligned} \epsilon_i &= (1 - s_i'' \lambda^q) / (\lambda^p - s_i' s_i'' \lambda^q) \\ \xi_i &= -s_i'' (1 - s_i' \epsilon_i) \\ \tau_i &= 1 / (s_i' \lambda^p - s_i'' \lambda^q). \end{aligned}$$

The integers $\{p, q\}$ can be related to any triangular shape through the Sine rule. The possible resolved triad shapes depend therefore on the combination of $\{\lambda, p, q\}$: For $\lambda \rightarrow 1$ any triad geometry may be constructed for large/small enough values of $\{p, q\}$, while for $\{\lambda, p, q\} = \{\varphi, 1, 2\}$ triads collapse to a line. Hence, for each chosen set of $\{\lambda, p, q\}$, the shell model consists, independently of scale k_n , only of fixed-shaped triad interactions.

The outer sums over all triad shapes in (5)–(6) are thus reduced to just three (fixed-shape) helical triad interactions per MTI-component per resolved scale k_n , exemplified in Figure 3 for the case of $i = 2$. Note that only $I_{n;i}^{uu}$ contains triad interactions of one MTI component exclusively, namely G_i^{uuu} . The remaining three ($I_{n;i}^{BB}$, $I_{n;i}^{uB}$, and $I_{n;i}^{Bu}$) contain a mix of the MHD interactions G_i^{uBB} , G_i^{BuB} and G_i^{BBu} .

The dissipation terms are defined as $D_n^u = \nu k_n^2 + \nu_L k^{-4}$ and $D_n^B = \eta k_n^2 + \eta_L k^{-4}$ where the drag terms, $\nu_L k^{-4}$ and $\eta_L k^{-4}$, are added the usual way to remove energy building up at large scales.

Like the ideal MHD equations (5)–(6), the MTI shell model also inviscidly conserves energy (E), magnetic helicity (H_M),

and cross-helicity (H_C), which can be shown by applying (14)–(15) to (2)–(4), telescoping sums, and inserting the boundary conditions $u_n^s, B_n^s = 0$ for $n < 0$ and $n > N$. Unlike the ideal MHD equations (5)–(6), however, the MTI shell model (14)–(15) conserves all MHD invariants only if the resolved MTIs are homochiral; that is, each MTI component must share the same sign group, i . Hence, the four possible shell model MTIs are $G_i^{uuu} + G_i^{uBB} + G_i^{BuB} + G_i^{BBu}$ for $i = 1, 2, 3, 4$.

4.1. Forcing terms

The kinematic (f_n^u) and magnetic (f_n^B) forcing terms may be constructed to allow full control over the pumping of energy ($\varepsilon = \varepsilon^u + \varepsilon^B$), kinematic helicity (δ^u), magnetic helicity (δ^B), and cross-helicity ($\gamma = \gamma^u + \gamma^B$), where the superscripts u and B refer to the injection fields. For the kinematic forcing term, this amounts to solving the forcing balance equations $\varepsilon^u = f_n^u u_n^{+,*} + f_n^u u_n^{-,*} + \text{c.c.}$, $\delta^u = k_n(f_n^u u_n^{+,*} - f_n^u u_n^{-,*} + \text{c.c.})$, $\gamma^u = f_n^u B_n^{+,*} + f_n^u B_n^{-,*} + \text{c.c.}$, and $0 = f_n^u B_n^{+,*} - f_n^u B_n^{-,*} + \text{c.c.}$. For the magnetic forcing term, f_n^B , the balance equations are similar but with u and B interchanged, with the exception that the balance of magnetic helicity is given by $\delta^B = k_n^{-1}(f_n^B B_n^{+,*} - f_n^B B_n^{-,*} + \text{c.c.})$. Solving these closed sets of equations, one finds

$$f_n^u = \frac{1}{2} \frac{(\varepsilon^u + s\delta^u/k_n)B_n^s - \gamma^u u_n^s}{u_n^{s,*} B_n^s - u_n^s B_n^{s,*}}$$

$$f_n^B = \frac{1}{2} \frac{(\varepsilon^B + s\delta^B k_n)u_n^s - \gamma^B B_n^s}{B_n^{s,*} u_n^s - B_n^s u_n^{s,*}},$$

which will provide a constant pumping of energy, kinematic helicity, magnetic helicity, and cross-helicity, for constant ε , δ^u , δ^B , and γ , respectively, thus allowing the simulated cascade partitionings to easily be normalized against the pumping rates.

4.2. Spectral energy flux

The total spectral flux of energy (kinetic+magnetic), carried by a homochiral MTI of sign group i through the k_n -th scale, is given by $\Pi_i(k_n) = d_{i|\text{nl.}} \sum_{m=0}^n (|u_m^+|^2 + |u_m^-|^2 + |B_m^+|^2 + |B_m^-|^2)$, where $d_{i|\text{nl.}}$ includes only the nonlinear terms in (14)–(15). Decomposing the total flux into the four separate MTI-component contributions, such that

$$\Pi_i(k_n) = \Pi_i^{uuu}(k_n) + \Pi_i^{uBB}(k_n) + \Pi_i^{BuB}(k_n) + \Pi_i^{BBu}(k_n),$$

requires isolating the terms in (14)–(15) corresponding to triad interactions G_i^{uuu} , G_i^{uBB} , G_i^{BuB} , and G_i^{BBu} , which can be shown

to give

$$G_i^{uuu} \begin{cases} d_{i|\text{nl.}} u_n^s = sk_n I_{n;i}^{uu} \left(1, \frac{\varepsilon_i}{\lambda^p}, \frac{\xi_i}{\lambda^q}\right) \\ d_{i|\text{nl.}} B_n^s = 0 \end{cases}$$

$$G_i^{uBB} \begin{cases} d_{i|\text{nl.}} u_n^s = -sk_n I_{n;i}^{BB} (1, 0, 0) \\ d_{i|\text{nl.}} B_n^s = -sk_n \left[I_{n;i}^{uB} (0, \tau_i, 0) + I_{n;i}^{uB} (0, 0, \tau_i) \right] \end{cases}$$

$$G_i^{BuB} \begin{cases} d_{i|\text{nl.}} u_n^s = -sk_n I_{n;i}^{BB} \left(0, \frac{\varepsilon_i}{\lambda^p}, 0\right) \\ d_{i|\text{nl.}} B_n^s = sk_n \left[I_{n;i}^{Bu} (0, 0, \tau_i) - I_{n;i}^{Bu} (\tau_i, 0, 0) \right] \end{cases}$$

$$G_i^{BBu} \begin{cases} d_{i|\text{nl.}} u_n^s = -sk_n I_{n;i}^{BB} \left(0, 0, \frac{\xi_i}{\lambda^q}\right) \\ d_{i|\text{nl.}} B_n^s = sk_n \left[I_{n;i}^{Bu} (\tau_i, 0, 0) + I_{n;i}^{Bu} (0, \tau_i, 0) \right] \end{cases}.$$

Using these MTI-decomposed equations, the component-wise fluxes follow as (telescoping sums and applying the boundary conditions $u_n^s, B_n^s = 0$ for $n < 0$ and $n > N$):

$$\Pi_i^{uuu}(k_n) = + \sum_{m=n+1}^{n+q} \Delta_{m;i}^{uuu} - s' \varepsilon_i \sum_{m=n+1}^{n+q-p} \Delta_{m;i}^{uuu} \quad (16)$$

$$\Pi_i^{uBB}(k_n) = - \sum_{m=n+1}^{n+q} \Delta_{m;i}^{uBB} + s' \lambda^p \tau_i \sum_{m=n+1}^{n+q-p} \Delta_{m;i}^{uBB} \quad (17)$$

$$\Pi_i^{BuB}(k_n) = -\tau_i \sum_{m=n+1}^{n+q} \Delta_{m;i}^{BuB} + s' \varepsilon_i \sum_{m=n+1}^{n+q-p} \Delta_{m;i}^{BuB} \quad (18)$$

$$\Pi_i^{BBu}(k_n) = +\tau_i \sum_{m=n+1}^{n+q} \Delta_{m;i}^{BBu} - s' \lambda^p \tau_i \sum_{m=n+1}^{n+q-p} \Delta_{m;i}^{BBu}, \quad (19)$$

where the triple correlators, $\Delta_{m;i}^{XYZ}$, are defined as

$$\Delta_{m;i}^{XYZ} = 2k_{m-q} \text{Re} \left[X_{m-q}^{+,*} Y_{m-q+p}^{s',*} Z_m^{s''} - X_{m-q}^{-,*} Y_{m-q+p}^{-s',*} Z_m^{-s''} \right].$$

5. NUMERICAL RESULTS

For each of the four homochiral MTIs, two different triad shapes (crosses in Figure 2) were considered in order to test the predicted behaviours of the MTI components. The model was configured using a shell spacing of $\lambda = 1.2$ with $\{p, q\} = \{1, 2\}$ and $\{p, q\} = \{3, 4\}$, corresponding to pseudo-invariant exponents of $\alpha^{BuB} = \{-2.0, +1.0\}$ and $\alpha^{BBu} = \{+8.8, +4.5\}$, respectively. The chosen triad shapes thus sample both the forward- and reverse-contributing parts of the space of triad geometries for G_i^{BuB} interactions (Figure 2a).

For simplicity, all model simulations were configured with identical free parameters (the values of which were found not to influence results): $\nu = \mu = 1 \times 10^{-8}$ (i.e. a magnetic Prandtl number of one), $\nu_L = \mu_L = 1 \times 10^1$, $k_0 = 1$, and $N = 76$. The modes u_n^s and B_n^s were initialized in a K41-scaling state $\sim k_n^{-2/3}$ (the shell model equivalent of $\sim k^{-5/3}$) with zero helicity of any kind, and stepped forward using a fourth-order Runge–Kutta integration scheme with a time-step of $\Delta t = 5 \times 10^{-7}$. The injection rates $\varepsilon^u = \varepsilon^B = 1/2$, and $\delta^u, \delta^B, \gamma = 0$ (i.e. no forcing handedness, elaborated on in the discussion) were evenly applied over p shells, starting from shell $n_f = 30$. Thus, in the $p = 3$ configuration, shells #31 and

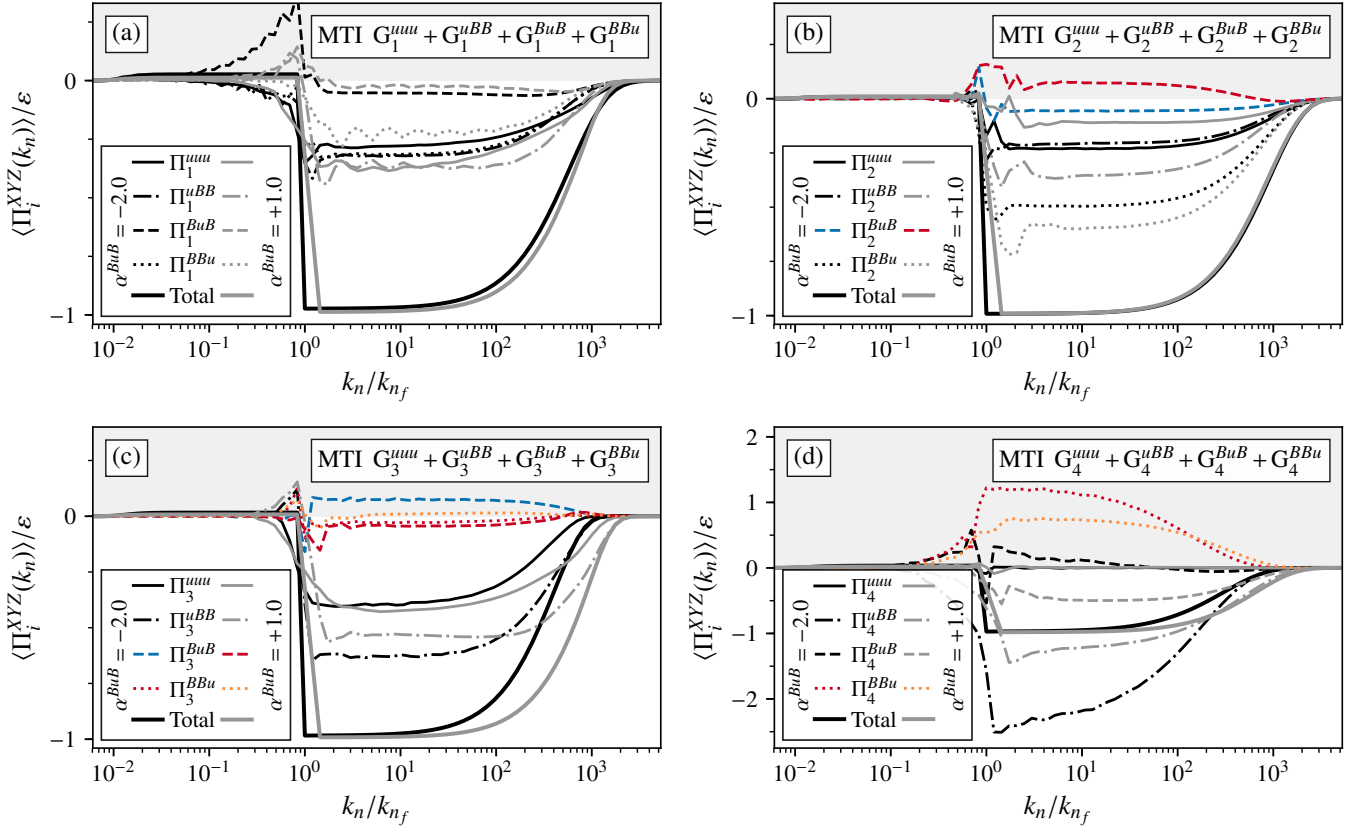


Figure 4. Simulated energy cascade partitioning among the four MTI components G_i^{uuu} , G_i^{uBB} , G_i^{BuB} , and G_i^{BBu} for each of the four possible homochiral MTIs $G_i^{uuu} + G_i^{uBB} + G_i^{BuB} + G_i^{BBu}$ ($i = 1, 2, 3, 4$) in panels a–d, respectively. The component-wise contributions are calculated using (16)–(19). Negative (positive) values correspond to forward/downscale (reverse/upscale) energy cascades contributions. Blue lines denote hypothesised forward cascade contributions according to the pseudo-invariant predictions, while red/orange lines denote hypothesised reverse contributions (interactions conserving an enstrophy-like quantity). Black/gray lines denote contributions by interactions not conserving any pseudo-invariants.

#32 are forced too. Note that while dynamo studies typically inject only kinematic energy, both kinematic and magnetic energy was injected in the present simulations. Although no difference in the energy cascade partitioning among MTI components is found for homochiral MTIs $i = 1, 2, 3$, the magnetic field collapses for $i = 4$ unless magnetic energy is injected.

The simulated energy cascade (nonlinear spectral flux) partitionings among MTI components for each of the four homochiral configurations $i = 1, 2, 3, 4$ are shown in figures 4a, 4b, 4c, and 4d, respectively, calculated using (16)–(19). The partitionings are shown for both triad shapes, labelled in the legends by the corresponding α^{BuB} -exponents. Gray/black lines represent components without additional pseudo-invariants, whereas components marked by coloured lines possess pseudo-invariants: blue colors indicate components for which the pseudo-invariant exponents are negative ($\alpha < 0$, hypothesised forward contribution), whereas red/orange colors mark components conserving enstrophy-like quantities with positive exponents ($\alpha > 0$, hypothesised reverse contribution).

Figures 4a and 4b show the energy cascade partitionings within homochiral MTIs $i = 1$ and $i = 2$ conform with the pseudo-invariant predictions: all MTI components contribute to a forward cascade, whereas the G_2^{BuB} component (conserving an enstrophy-like quantity, $\alpha^{BuB} > 0$) contributes to a reverse cascade.

Figure 4c shows the cascade partitioning within MTI $i = 3$ almost behaving as expected: all components contribute to a forward cascade, except for the G_3^{BuB} and G_3^{BBu} components which have their behaviours reversed — i.e. components conserving enstrophy-like quantities are found to contribute to a forward cascade and vice-versa.

Finally, Figure 4d shows the partitioning within MTI $i = 4$ also conforms with predictions: all components contribute to a forward cascade, whereas the G_4^{BBu} component (conserving an enstrophy-like quantity, $\alpha^{BBu} > 0$) contributes to a reverse cascade. For the simulated triad shape corresponding to $\alpha^{BuB} = -2.0$, however, the G_4^{BuB} component carries a small reverse contribution in spite of not conserving any enstrophy-like quantity.

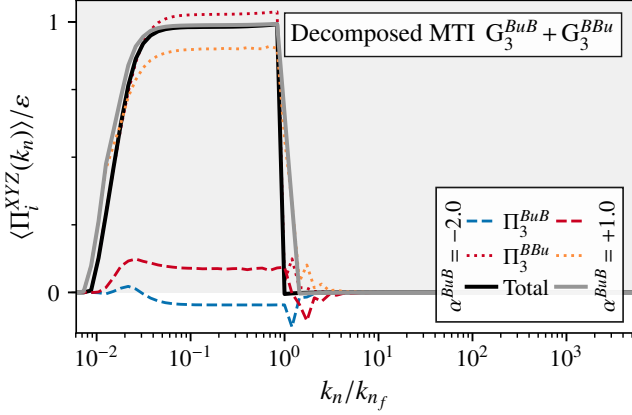


Figure 5. Simulated energy cascade partitioning among the two MTI components G_3^{BuB} and G_3^{BBu} in the decomposed MTI $G_3^{BuB} + G_3^{BBu}$. Negative (positive) values correspond to forward/downscale (reverse/upscale) energy cascades contributions. Blue lines denote hypothesised forward cascade contributions according to the pseudo-invariant predictions, while red/orange lines denote hypothesised reverse contributions (interactions conserving an enstrophy-like quantity).

6. DISCUSSION

The simulated energy cascade partitionings among the four MTI components demonstrate the influence of the new pseudo-invariants, which allow the partitionings to be understood in terms of conserved quantities in analogy to enstrophy in 2D HD turbulence. The implications for more realistic triad configurations (multi-MTI configurations) is however not immediately clear, and direct numerical simulations of (5)–(6) would ideally be needed to settle the general relevance of the partial MHD invariants.

The present simulations of homochiral MTIs of sign groups $i = 3$ and $i = 4$ suggest that coupling-induced effects, caused by the coupling of MTI components, might play an important role by altering the component-wise behaviours compared to the predictions based on the new partial invariants. To examine this possibility closer, we considered 4 additional simulations in which only G_i^{BuB} and G_i^{BBu} are coupled (i.e. decomposing the MTIs by disregarded G_i^{uuu} and G_i^{uBB} interactions, thereby conserving only energy and the pseudo-invariants). Using the same model configuration as above, Figure 5 shows the resulting partitionings among the two components G_3^{BuB} and G_3^{BBu} in the decomposed MTI $G_3^{BuB} + G_3^{BBu}$ (decomposed MTIs $i = 1, 2, 4$ are not shown). For all decomposed MTIs, the component-wise behaviours are found to conform with the pseudo-invariant predictions, suggesting discrepancies between the full and decomposed MTIs might indeed be due to coupling-induced effects (i.e. interactions between MTI components).

The partitioning of the energy cascade between symmetrized helical triad interactions was recently investigated

by Alexakis (2017) in a direct numerical simulation of the spectral-helical Navier–Stokes equation. Like here, it was found that the energy cascade partitions itself into approximately constant-flux components within the inertial range, an intriguing result given that only the total energy flux is required to be constant. Moreover, Alexakis (2017) found that the partitioning was unaffected by the pumping of kinematic helicity, suggesting the partitioning might be universal (among a given set of resolved triads). If so, the physical explanation for the directionalities of the different embedded energy cascades in terms of partial invariants might be applicable in a general, forcing-independent sense.

Inspired by this result, we conducted additional simulations where the four homochiral MTIs were forced with kinematic helicity (δ^u), magnetic helicity (δ^B) and cross-helicity (γ) besides energy, in contrast to the non-helical forcing used above ($\delta^u, \delta^B, \gamma = 0$). While the partitionings were found to be independent of δ^u and δ^B , suggesting the partitionings might be universal, the same was not found for a nonzero injection of cross-helicity ($\gamma \neq 0$). This is exemplified in Figure 6 for the homochiral MTI $i = 1$ (similar results were found for $i = 2, 3, 4$), demonstrating the divergent, non-constant flux components which develop in the case of $\gamma^u = 0.25$. Note that when pumping cross-helicity, the simulated directionalities of the embedded cascade contributions do generally not agree with the pseudo-invariant predictions — e.g. in Figure 6, all components are predicted to contribute to a forward cascade since no enstrophy-like quantities are conserved.

Because the evolution of magnetic modes depend on the alignment between velocity and magnetic modes (cross-helicity) according to (6), it is not entirely surprising that injecting cross-helicity can affect the detailed partitioning. Note that this result is in agreement with a linear stability

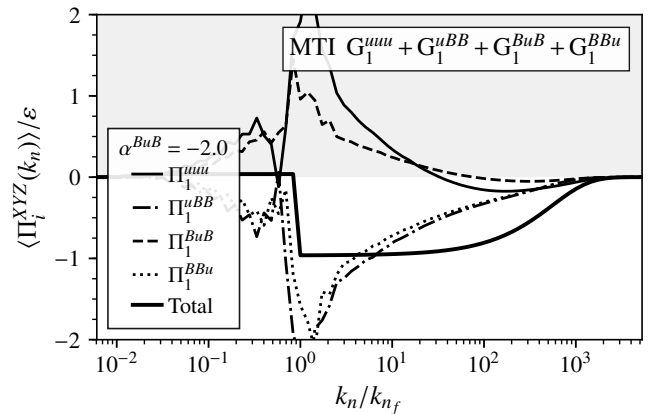


Figure 6. Simulated energy cascade partitioning among the four MTI components within the homochiral MTI $G_1^{uuu} + G_1^{uBB} + G_1^{BuB} + G_1^{BBu}$ for a nonzero cross-helicity pumping of $\gamma^u = 0.25$. Negative (positive) values correspond to forward/downscale (reverse/upscale) energy cascades contributions.

analysis which too predicts that triad leg (modal) stabilities depend on velocity–magnetic alignments (Linkmann et al. 2016).

The present analysis considered only a magnetic Prandtl number of $Pr_m = 1$. While investigating large and small magnetic Prandtl number flows is out of scope of the present work, studies such as Verma & Kumar (2016) indicate that under some forcing conditions, the partitioning might be unaffected (although helically decomposed dynamics were not considered in their study). Extending this work to other Pr_m would, however, be of great interest in order to cast more light on the reverse, upscale turbulent transfer of magnetic energy in small and large Pr_m turbulence with implications for solar/planetary dynamos and interstellar dynamos, respectively.

7. CONCLUSION

In conclusion, we proposed an explanation for the behaviours of the elementary three-wave (triad) interactions in spectral-helically decomposed ideal MHD turbulence in terms of partially conserved quantities. By showing a subset of helical triad interactions conserve new enstrophy-like quantities, we conjecture that these interactions might contribute to embedded, inverse energy cascades developing in ideal three-dimensional MHD turbulence in analogy to enstrophy-conserving triad interactions in two-dimensional hydrodynam-

ical (HD) turbulence. Because the largest scale involved in the enstrophy-like-conserving triad interactions is associated with the magnetic field, we note that such interactions might lead to an inverse (upscale) transfer of magnetic energy.

In order to test the predictions based on the new partial invariants (pseudo-invariants), we introduced a helically decomposed reduced wave-space model (shell model). By conducting numerical simulations of the four kinds of homochiral minimal sets of triad interactions (MTIs) (minimal in the sense of being required to conserve the ideal MHD invariants), we demonstrated the usefulness of the partial invariants for understanding the resulting energy cascade contributions within each MTI. Importantly, however, we note that the injection of cross-helicity by the forcing mechanism, and the effect of coupling certain types of MTI components (i.e. triads), might complicate the result. Further direct numerical simulations are therefore needed to settle the discrepancies and to establish the general role of pseudo-invariants in turbulent MHD cascade dynamics.

While this study for simplicity was limited to consider only a magnetic Prandtl number of $Pr_m = 1$, the prospects of embedded, inverse magnetic energy cascades in ideal MHD turbulence due to partial invariants has potential intriguing implications for both large and small Pr_m turbulent dynamos, relevant for the evolution of solar/planetary and interstellar magnetic fields, respectively.

REFERENCES

- Alexakis, A. 2017, *Journal of Fluid Mechanics*, 812, 752
- Alexakis, A., Mininni, P. D., & Pouquet, A. 2006, *The Astrophysical Journal*, 640, 335
- Benzi, R., Biferale, L., Kerr, R., & Trovatore, E. 1996, *Physical Review E*, 53, 3541
- Biferale, L., Musacchio, S., & Toschi, F. 2012, *Physical review letters*, 108, 164501
- Biskamp, D. 1993, *Nonlinear magnetohydrodynamics*, volume 1 of *Cambridge Monographs on Plasma Physics*, Cambridge University Press, Cambridge
- Boffetta, G., & Musacchio, S. 2010, *Physical Review E*, 82, 016307
- Boldyrev, S. 2005, *The Astrophysical Journal Letters*, 626, L37
- Brandenburg, A., & Subramanian, K. 2005, *Physics Reports*, 417, 1
- Brissaud, A., Frisch, U., Léorat, J., Lesieur, M., & Mazure, A. 1973, *Physics of Fluids (1958-1988)*, 16, 1366
- Constantin, P., & Majda, A. 1988, *Communications in mathematical physics*, 115, 435
- De Pietro, M., Biferale, L., & Mailybaev, A. A. 2015, *Phys. Rev. E*, 92, 043021, doi: [10.1103/PhysRevE.92.043021](https://doi.org/10.1103/PhysRevE.92.043021)
- De Pietro, M., Mailybaev, A. A., & Biferale, L. 2017, *Physical Review Fluids*, 2, 034606
- Ditlevsen, P. D., & Giuliani, P. 2001a, *Physics of Fluids (1994-present)*, 13, 3508
- . 2001b, *Physical Review E*, 63, 036304
- Frisch, U., Pouquet, A., Léorat, J., & Mazure, A. 1975, *Journal of Fluid Mechanics*, 68, 769
- Gürçan, Ö. 2017, *Physical Review E*, 95, 063102
- . 2018, *Physical Review E*, 97, 063111
- Iroshnikov, P. 1964, *Soviet Astronomy*, 7, 566
- Kraichnan, R. H. 1973, *Journal of Fluid Mechanics*, 59, 745
- Krause, F., & Rädler, K. 1980, *Akademie-Verlag*, Berlin
- Lessinnes, T., Plunian, F., & Carati, D. 2009, *Theoretical and Computational Fluid Dynamics*, 23, 439
- Lessinnes, T., Plunian, F., Stepanov, R., & Carati, D. 2011, *Physics of Fluids (1994-present)*, 23, 035108
- Linkmann, M., Berera, A., McKay, M., & Jäger, J. 2016, *Journal of Fluid Mechanics*, 791, 61
- Linkmann, M., & Dallas, V. 2016, *Physical Review E*, 94, 053209
- . 2017, *Physical Review Fluids*, 2, 054605
- Linkmann, M., Sahoo, G., McKay, M., Berera, A., & Biferale, L. 2017, *The Astrophysical Journal*, 836, 26
- Matthaeus, W. H., & Zhou, Y. 1989, *Physics of Fluids B: Plasma Physics*, 1, 1929

- Mininni, P. D., Alexakis, A., & Pouquet, A. 2009, *Physics of Fluids* (1994-present), 21, 015108
- Mininni, P. D., & Pouquet, A. 2013, *Physical Review E*, 87, 033002
- Moffatt, H. K. 1969, *Journal of Fluid Mechanics*, 35, 117
- . 1978, Cambridge University Press, Cambridge, London, New York, Melbourne
- Monthus, C. 2018, arXiv preprint arXiv:1810.05082
- Plunian, F., Stepanov, R., & Frick, P. 2013, *Physics Reports*, 523, 1
- Pouquet, A., Frisch, U., & Léorat, J. 1976, *Journal of Fluid Mechanics*, 77, 321
- Rathmann, N. M., & Ditlevsen, P. D. 2016, *Phys. Rev. E*, 94, 033115, doi: [10.1103/PhysRevE.94.033115](https://doi.org/10.1103/PhysRevE.94.033115)
- . 2017, *Physical Review Fluids*, 2, 054607
- Sahoo, G., De Pietro, M., & Biferale, L. 2017, *Physical Review Fluids*, 2, 024601
- Steenbeck, M., Krause, F., & Rädler, K.-H. 1966, *Zeitschrift für Naturforschung A*, 21, 369
- Stepanov, R., Frick, P., & Mizeva, I. 2014, *The Astrophysical Journal Letters*, 798, L35
- . 2015, *The Astrophysical Journal Letters*, 798, L35
- Sulem, P., She, Z. S., Scholl, H., & Frisch, U. 1989, *Journal of Fluid Mechanics*, 205, 341
- Verma, M. K., & Kumar, R. 2016, *Journal of Turbulence*, 17, 1112
- Waleffe, F. 1992, *Physics of Fluids A: Fluid Dynamics* (1989-1993), 4, 350